Guided modes and loss in a plasma-filled Bragg waveguide

J. D. Chatterton and J. L. Shohet[a)]
Plasma Processing and Technology Laboratory and Department of Electrical and Computer Engineering, University of Wisconsin-Madison, Madison, Wisconsin 53706, USA

(Received 6 June 2007; accepted 17 July 2007; published online 24 September 2007)

The dispersion and radiation loss of propagating modes in a plasma-filled Bragg waveguide are investigated. The Bragg waveguide at a center frequency of 10 GHz is modeled with the transfer-matrix method, which has been used to analyze optical Bragg fibers. We calculate the dispersion and radiation loss of the TE_{01}, TM_{01}, and HE_{11} modes and show how they vary as a function of plasma density. As the plasma density inside the waveguide increases, the cutoff frequency of each mode increases. An increase in plasma density increases the radiation loss in the TE_{01} mode while it decreases the radiation loss in the TM_{01} mode; the effect on the HE_{11} mode is to increase the radiation loss for frequencies above 10.2 GHz and decrease the radiation loss for frequencies below 10.2 GHz. © *2007 American Institute of Physics*. [DOI: 10.1063/1.2776374]

I. INTRODUCTION AND BACKGROUND

A Bragg waveguide is a dielectric waveguide that is constructed of alternating dielectric layers of differing thickness and indices of refraction,[1] as shown in Fig. 1. In the optical portion of the spectrum, Bragg waveguides have been constructed for optical fibers and have been shown to have low loss and excellent mode discrimination.[2–5] Previous analysis of these optical Bragg fibers have shown that with a sufficient number of layers (approximately 17), radiation loss can be reduced to 0.01 dB/km for the TE_{01} mode. For a given frequency, this radiation loss has also been shown to decrease as the radius of the optical fiber increases.[2]

Depending of the application of the optical fiber, such low radiation loss might not be required. Optical fibers with loss on the order of 1 dB/cm have been fabricated out of Si/Si_3N_4 with only 8 dielectric layers.[6] The analysis of these optical fibers, however, was done only for radiation in the optical band and under the assumption that the fibers were hollow.

In this work, we investigate the behavior of the modes of a plasma-filled Bragg waveguide in the gigahertz portion of the spectrum. Such waveguides can be used for spectroscopic measurements of small diameter plasmas.

Although the methods used in this work can be applied to any mode, for simplicity we limit the calculations to the TE_{01}, TM_{01}, and the HE_{11} hybrid modes. We calculate the dispersion, loss, and field structure for each mode and determine how these parameters change when a uniform plasma of variable density fills the center region of the waveguide.

II. THEORY

The basic structure of a Bragg waveguide is shown in Fig. 1. In its most general form, a Bragg waveguide consists of a central core surrounded by a multilayer cladding region that consists of alternating dielectric layers of high and low indices of refraction. In Fig. 1, the high and low layers are shown in black and gray, respectively. The high-K layer is adjacent to the core region, and the number of high-K and low-K layers are equal.

The mode structure in a Bragg waveguide can be calculated by employing the transfer-matrix method.[1] For a guided-wave solution in the hth dielectric layer in a cylindrical coordinate system, the longitudinal fields take the following form:[7]

$$E_{z,h}(r,\phi,z) = [A_{nmh}J_m(k_{nmh}r) + B_{nmh}Y_m(k_{nmh}r)]e^{jm\phi}e^{j\beta z},$$

$$H_{z,h}(r,\phi,z) = [C_{nmh}J_m(k_{nmh}r) + D_{nmh}Y_m(k_{nmh}r)]e^{jm\phi}e^{j\beta z}, \quad (1)$$

where $k_{nmh}=\sqrt{\varepsilon_h\omega^2/c^2-\beta_{nm}^2}$, ω is the radian frequency, β_{nm} is the longitudinal wave number, n is the radial mode number, m is the azimuthal mode number, A_{nmh}, B_{nmh}, C_{nmh}, and D_{nmh} are constant amplitude coefficients within the hth dielectric layer and J_m and Y_m are Bessel functions of the first and second kind, respectively. Here ε_h, the permittivity of the hth layer, can be complex, with the imaginary part accounting for dissipation within the layer if any.[8] In this work, for simplicity we consider the permittivity of each layer to be real, as it has been found previously that the radiation loss and dispersion do not depend heavily on the imaginary part of a complex permittivity,[8] if it is small compared to the real part.

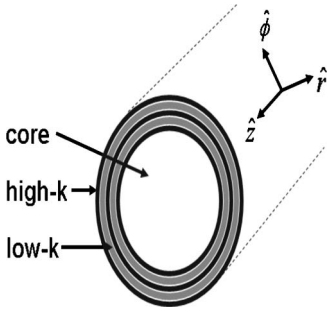

FIG. 1. Bragg fiber.

[a)]Electronic mail: shohet@engr.wisc.edu

From the longitudinal field components, all other field components can be found as shown below[7]

$$E_{r,h}(r,\phi,z) = \frac{-j\beta}{k_c^2}\left[\frac{\partial E_z}{\partial r} + \frac{\omega\mu}{\beta r}\frac{\partial H_z}{\partial \phi}\right], \tag{2}$$

$$E_{\phi,h}(r,\phi,z) = \frac{j\beta}{k_c^2}\left[-\frac{\partial E_z}{r\,\partial \phi} + \frac{\omega\mu}{\beta}\frac{\partial H_z}{\partial r}\right], \tag{3}$$

$$H_{r,h}(r,\phi,z) = \frac{j}{k_c^2}\left[\frac{\omega\varepsilon}{r}\frac{\partial E_z}{\partial \phi} - \beta\frac{\partial H_z}{\partial r}\right], \tag{4}$$

and

$$H_{\phi,h}(r,\phi,z) = \frac{-j}{k_c^2}\left[\omega\varepsilon\frac{\partial E_z}{\partial r} + \frac{\beta}{r}\frac{\partial H_z}{\partial \phi}\right]. \tag{5}$$

This representation allows us to write a matrix expression for the field components in a given dielectric layer in terms of the longitudinal-field components in that particular layer. This expression is[8]

$$\begin{bmatrix} E_{z,h} \\ H_{\phi,h} \\ H_{z,h} \\ E_{\phi,h} \end{bmatrix} = M_h(r)\begin{bmatrix} A_{nmh} \\ B_{nmh} \\ C_{nmh} \\ D_{nmh} \end{bmatrix}, \tag{6}$$

where

$$M_h(r) = \begin{bmatrix} J_m(k_{nmh}r) & Y_m(k_{nmh}r) & 0 & 0 \\ \dfrac{-j\omega\varepsilon_0\varepsilon_n}{k_{nmh}}J'_m(k_{nmh}r) & \dfrac{-j\omega\varepsilon_0\varepsilon_n}{k_{nmh}}Y'_m(k_{nmh}r) & \dfrac{m\beta}{(k_{nmh})^2 r}J_m(k_{nmh}r) & \dfrac{m\beta}{(k_{nmh})^2 r}Y_m(k_{nmh}r) \\ 0 & 0 & J_m(k_{nmh}r) & Y_m(k_{nmh}r) \\ \dfrac{m\beta}{(k_{nmh})^2 r}J_m(k_{nmh}r) & \dfrac{m\beta}{(k_{nmh})^2 r}Y_m(k_{nmh}r) & \dfrac{-j\omega\mu_0}{k_{nmh}}J'_m(k_{nmh}r) & \dfrac{-j\omega\mu_0}{k_{nmh}}Y'_m(k_{nmh}r) \end{bmatrix}. \tag{7}$$

At the interface of any two dielectric layers, the boundary conditions for the tangential field components must be satisfied. That is, the longitudinal (E_z, H_z) and azimuthal (E_ϕ, H_ϕ) fields must be continuous across each dielectric boundary. If any surface currents exist due to the complex permittivity of a dielectric layer, they are assumed to be negligible. Thus, a relationship can be expressed between the amplitude coefficients in the hth layer and the amplitude coefficients in the $(h+1)$th layer which is

$$M_{h+1}(\rho_h)\begin{bmatrix} A_{nmh+1} \\ B_{nmh+1} \\ C_{nmh+1} \\ D_{nmh+1} \end{bmatrix} = M_h(\rho_h)\begin{bmatrix} A_{nmh} \\ B_{nmh} \\ C_{nmh} \\ D_{nmh} \end{bmatrix}, \tag{8}$$

where ρ_h is the radius of the interface between the hth and $(h+1)$th dielectric layer and M_h and M_{h+1} are defined according to Eq. (7) above.[8] This can be rearranged into an expression for the amplitude coefficients in the $(h+1)$th layer as shown below

$$\begin{bmatrix} A_{nmh+1} \\ B_{nmh+1} \\ C_{nmh+1} \\ D_{nmh+1} \end{bmatrix} = [M_{h+1}(\rho_h)]^{-1} M_h(\rho_h)\begin{bmatrix} A_{nmh} \\ B_{nmh} \\ C_{nmh} \\ D_{nmh} \end{bmatrix}, \tag{9}$$

where $[M_{h+1}]^{-1}$ is the inverse of M_{h+1} which has the form

$$[M_{h+1}]^{-1} = \frac{1}{d}\begin{bmatrix} Y'_m(k_{nmh}r) & \dfrac{-jk_{nmh}Y_m(k_{nmh}r)}{\omega\varepsilon_h} & \dfrac{jm\beta_{mn}Y_m(k_{nmh}r)}{\omega k_{nmh}r\varepsilon_h} & 0 \\ -J'_m(k_{nmh}r) & \dfrac{jk_{nmh}J_m(k_{nmh}r)}{\omega\varepsilon_h} & \dfrac{-jm\beta_{mn}J_m(k_{nmh}r)}{\omega k_{nmh}r\varepsilon_h} & 0 \\ \dfrac{jm\beta_{mn}Y_m(k_{nmh}r)}{\omega k_{nmh}r\mu_0} & 0 & Y'_m(k_{nmh}r) & \dfrac{-jk_nY_m(k_{nmh}r)}{\omega\mu_0} \\ \dfrac{-jm\beta_{mn}J_m(k_{nmh}r)}{\omega k_{nmh}r\mu_0} & 0 & -J'_m(k_{nmh}r) & \dfrac{jk_{nmh}J_m(k_{nmh}r)}{\omega\mu_0} \end{bmatrix}, \tag{10}$$

and where

$$d = J_m(k_{nmh}r)Y'_m(k_{nmh}r) - Y_m(k_{nmh}r)J'_m(k_{nmh}r). \tag{11}$$

We have assumed that the fields in all the layers inside the waveguide including the central core consist of radial standing waves. That is, the waves do not propagate in the radial direction. However, in relating the fields outside the Bragg waveguide to the fields inside the last dielectric layer, we choose to exchange the radial standing-wave solution of the cylindrical wave equation given in Eq. (1) for a solution that represents radial traveling waves, which is given by

$$E_z = [A_{outside}H_m^2(k_{nm0}r) + B_{outside}H_m^1(k_{nm0}r)]e^{jm\phi}e^{j\beta z},$$

$$H_z = [C_{outside}H_m^2(k_{nm0}r) + D_{outside}H_m^1(k_{nm0}r)]e^{jm\phi}e^{j\beta z}, \tag{12}$$

where $k_{nm0} = \sqrt{\varepsilon_0\omega^2/c^2 - \beta_{nm}^2}$, $H_m^1(k_{nmh}r)$ is the Hankel function of the first kind of order m that represents a radially inward propagating wave, and $H_m^2(k_{nmh}r)$ is the Hankel function of the second kind that represents a radially outward propagating wave.[9]

Thus, for the fields outside the fiber, M takes a different form, which we represent as N_0

$$N_0(r) = \begin{bmatrix} H_m^2(k_{nm0}r) & H_m^1(k_{nm0}r) & 0 & 0 \\ \frac{-j\omega\varepsilon_0}{k_{nm0}}H_m'^2(k_{nm0}r) & \frac{-j\omega\varepsilon_0}{k_{nm0}}H_m'^1(k_{nm0}r) & \frac{m\beta_{nm}}{(k_{nm0})^2r}H_m^2(k_{nm0}r) & \frac{m\beta_{nm}}{(k_{nm0})^2r}H_m^1(k_{nm0}r) \\ 0 & 0 & H_m^2(k_{mn}^0r) & H_m^1(k_{nm0}r) \\ \frac{m\beta_{nm}}{(k_{nm0})^2r}H_m^2(k_{nm0}r) & \frac{m\beta_{nm}}{(k_{nm0})^2r}H_m^1(k_{nm0}r) & \frac{-j\omega\mu_0}{k_{nm0}}H_m'^2(k_{nm0}r) & \frac{-j\omega\mu_0}{k_{nm0}}H_m'^1(k_{nm0}r) \end{bmatrix}. \tag{13}$$

Equation (8) can then be modified for the last boundary as

$$N_0(\rho_h)\begin{bmatrix} A_{outside} \\ B_{outside} \\ C_{outside} \\ D_{outside} \end{bmatrix} = M_h(\rho_h)\begin{bmatrix} A_{nmh} \\ B_{nmh} \\ C_{nmh} \\ D_{nmh} \end{bmatrix}, \tag{14}$$

which now gives a relationship between the fields outside the Bragg waveguide and the fields inside the last dielectric layer.

By applying Eq. (9) successively from the core outwards and applying Eq. (14) to relate the fields outside the waveguide to the fields inside the waveguide, the amplitude coefficients outside of the Bragg waveguide can be related to the amplitude coefficients within the core region by a 4×4 transfer matrix[8]

$$\begin{bmatrix} A_{outside} \\ B_{outside} \\ C_{outside} \\ D_{outside} \end{bmatrix} = \begin{bmatrix} t_{11} & t_{12} & t_{13} & t_{14} \\ t_{21} & t_{22} & t_{23} & t_{24} \\ t_{31} & t_{32} & t_{33} & t_{34} \\ t_{41} & t_{42} & t_{43} & t_{44} \end{bmatrix}\begin{bmatrix} A_{core} \\ B_{core} \\ C_{core} \\ D_{core} \end{bmatrix}. \tag{15}$$

Two additional boundary conditions are now enforced. First, the fields in the core region must be finite. This requires that $B_{core}=D_{core}=0$ since Bessel functions of the second kind, $Y_m(x)$, are infinite when their argument is zero. Second, the cylindrical electromagnetic waves outside the waveguide must consist only of outwardly propagating waves.[9] Physically, this corresponds to having no sources or points of reflection located outside of the waveguide. This requires that $B_{outside}=D_{outside}=0$.

By application of these additional boundary conditions, Eq. (15) can then be written as

$$B_{outside} = t_{21}A_{core} + t_{23}C_{core} = 0,$$

$$D_{outside} = t_{41}A_{core} + t_{43}C_{core} = 0, \tag{16}$$

which can be expressed as

$$\begin{bmatrix} t_{21} & t_{23} \\ t_{41'} & t_{43} \end{bmatrix}\begin{bmatrix} A_{core} \\ C_{core} \end{bmatrix} = 0. \tag{17}$$

By specifying the physical dimensions and permittivities of the dielectric layers of the waveguide and choosing a given frequency and azimuthal mode number, the transfer matrix in Eq. (17) above becomes a function only of the longitudinal wave number β_{nmh}.[2] A solution for the system of equations exists when the determinant of the transfer matrix in Eq. (17) is zero. A search for values of β_{nm} that makes the determinant in Eq. (17) zero can be done numerically. That is, we solve

$$\det(\mathbf{T}) = 0, \quad \mathbf{T} = \begin{bmatrix} t_{21} & t_{23} \\ t_{41} & t_{43} \end{bmatrix}. \tag{18}$$

With an infinite number of cladding layers, the modes would be completely confined and β, which is constant throughout the core and cladding regions, would be real.[2] However, with a finite number of cladding layers, β_{nm} is complex, with the imaginary part accounting for the radiation loss in the region outside of the guide for that mode. Once β_{nm} has been found, this value can be substituted into Eq. (17) to solve for the field amplitude coefficients in the core region. Once these have been found, Eq. (9) gives the field amplitude coefficients in each successive layer in terms of the core field amplitudes.

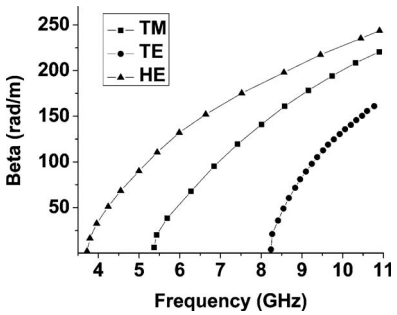

FIG. 2. Vacuum-core mode dispersion.

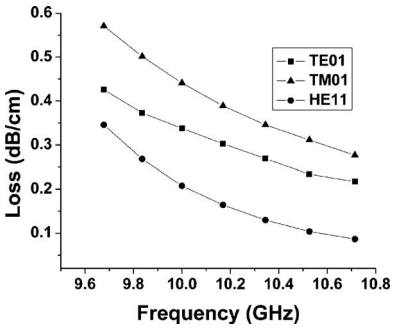

FIG. 3. Vacuum-core radiation loss.

III. RESULTS AND DISCUSSION

A. Vacuum core

Based on the previous development, we investigate the waveguide modes for a Bragg waveguide operating between 9.6 GHz and 10.4 GHz. This range was chosen because this range of frequencies can be utilized for molecular spectroscopy of plasmas present in the Bragg waveguide. The waveguide consists of eight alternating dielectric layers (four cladding pairs) of alternating refractive indices (K) of 2.4 and 1.7, which corresponds to Corning Macor and polymethyl methacrylate, respectively,[10] with the Corning Macor layer adjacent to the core. While the number of dielectric layers can be chosen arbitrarily in order to satisfy desired loss requirements, the individual thicknesses of the high-K and low-K layers were chosen such that the sum of the two thicknesses is approximately a quarter of a wavelength in thickness at 10 GHz. This quarter-wave condition has been employed at optical frequencies[2,3,8] and has been shown to result in low radiation loss for a given design frequency. The quarter-wave dimension in previous work was done such that the high-K layer was approximately 30% of the total thickness, while the low-K layer was approximately 70% of the total thickness.[8] With these considerations in mind, one cladding high/low index pair was chosen to be 7.5 mm thick, with the high-K layer and low-K layer having thicknesses of 2.25 mm and 5.25 mm, respectively. The radius of the core region was set to 2.5 cm in order to limit the number of propagating modes for the frequency range of interest and to allow a plasma of these dimensions to be used.

Initial calculations were made with the core region set to vacuum. Subsequently, these results were compared with a core region that was filled with a uniform collisionless plasma which implies an index of refraction that is less than 1.

Figure 2 shows the dispersion diagrams of the TE_{01}, TM_{01}, and HE_{11} modes for this waveguide. As can be seen in the figure, the HE_{11} mode has the lowest cutoff frequency, followed by the TM_{01} and the TE_{01} modes. This is in agreement with the behavior of such modes in a hollow cylindrical metallic waveguide, where the HE_{11} mode in the Bragg waveguide reduces to the TE_{11} mode in the metallic waveguide.[2] This relationship can be seen by examining the z components of the electric and magnetic fields. For the TE_{11} mode of the metallic waveguide, the z component of the electric field is zero. For a dielectric waveguide, the hybrid HE_{11} mode is the mode whose z component of the magnetic field is larger than the z component of the electric field.

Figure 3 shows the radiation loss of the TE_{01}, TM_{01}, and HE_{11} modes with the core region vacuum. As expected, at each frequency, the TM_{01} mode shows higher radiative loss than the TE_{01} mode[2] and the HE_{11} mode shows lower loss than the TE_{01} mode. This has also been shown to be the case at optical frequencies when the radius of the waveguide approaches the dimensions of the free-space wavelength.[8]

B. Plasma-filled core

We now investigate the dispersion, loss, and field structure of the same modes when a plasma is introduced into the core region. The core is assumed to be filled with a uniform cylindrical collisionless unmagnetized plasma. To represent this, we use the following expression for the plasma permittivity:

$$\varepsilon_p = \varepsilon_0\left(1 - \frac{\omega_p^2}{\omega^2}\right), \tag{19}$$

where ω_p is the plasma frequency which is related to the electron density of the plasma as

$$\omega_p = \sqrt{\frac{Ne^2}{m\varepsilon_0}}, \tag{20}$$

where N is the electron density, e is the charge of the electron, m is the mass of the electron, and ε_0 is the permittivity of free space. As can be seen from Eq. (19), the refractive index of the core region, which is the square root of the relative permittivity, decreases as the plasma density increases. By using a complex permittivity, collisions may be included in the calculations if desired.

Figure 4 shows how the dispersion of the TE_{01} mode changes as a function of the refractive index of the core. As the plasma density in the core increases, the cutoff frequency for the mode also increases. This behavior is not unexpected, because for a hollow cylindrical metallic waveguide, the cutoff frequency of the TE_{01} mode is given by

$$f_c = \frac{0.609}{a\sqrt{\mu\varepsilon}}, \tag{21}$$

where a is the radius of the waveguide.[7] Thus, for an increase in plasma density (a decrease in permittivity), we would expect the cutoff frequency to increase.

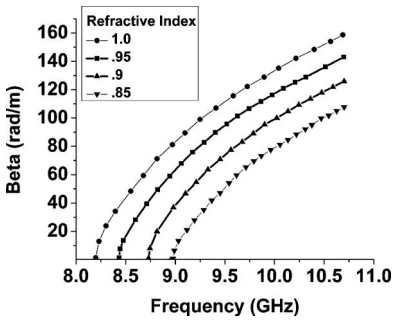

FIG. 4. Dispersion of the TE_{01} mode.

Figure 5 shows how the TE_{01} mode radiative loss changes as a function of the refractive index of the core. As can be seen in the figure, the loss increases as the refractive index of the core decreases. Moreover, as the plasma density increases, the loss at frequencies lower than 10 GHz increases at a higher rate. This behavior is not unexpected, as in previous work,[3,8] it has been shown that the loss for a given mode is dependent on the fiber parameters (number of cladding pairs and core radius) and that changing these parameters does not result in a linear change in the radiative loss. Likewise, we would not expect that changing the refractive index of the core region would result in a linear change in radiative loss for the mode.

The graphs in Fig. 6 show how the azimuthal component of the electric field for the TE_{01} mode varies as a function of refractive index of the core region. As expected, in making the comparison to a hollow cylindrical metallic waveguide, the azimuthal field amplitude is nearly zero at the first cladding interface, and then oscillates within further cladding layers. While there is not much discernable difference in the plots, the average value of the amplitude in the cladding region increases as the refractive index of the core decreases. This indicates a higher radiative loss since the radiation loss is proportional to the square of the field amplitude in the cladding.

In Fig. 7, the dispersion of the TM_{01} mode is plotted as a function of the relative index of the core. As with the TE_{01} mode, the cut-off frequency increases as the plasma density increases. Again, this can be compared to the cutoff behavior of the TM_{01} mode in a hollow cylindrical metallic waveguide, which is given by the expression

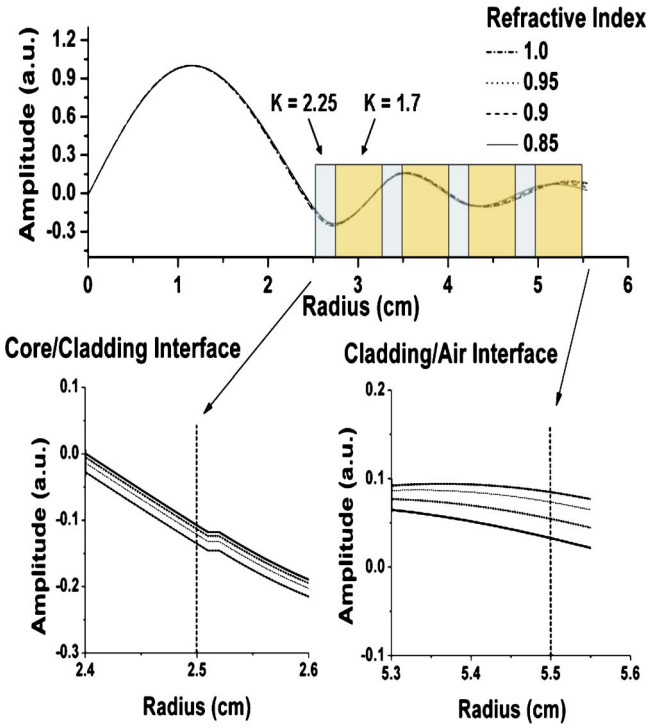

FIG. 6. (Color online) TE_{01} Azimuthal electric field amplitudes. The lower plots show a magnified view of the core/first cladding layer interface and the last cladding layer/air interface. The dielectric layers are indicated in color and their relative permittivity values are given.

$$f_c = \frac{0.383}{a\sqrt{\mu\varepsilon}}, \tag{22}$$

where f_c is the cut-off frequency and a is the radius of the waveguide.[7] As the plasma density increases, we would expect to see an increase in cut-off frequency.

Figure 8 shows how the TM_{01} radiation loss changes as a function of the refractive index of the core region. As was mentioned previously, the TM_{01} mode experiences higher losses compared to the TE_{01} mode when the core refractive index is 1. This behavior changes, however, as the refractive index of the core region decreases. When the refractive index of the core region decreases to 0.9, the TE_{01} mode is lossier than the TM_{01} mode for frequencies lower than 10.3 GHz. At frequencies higher than 10.3 GHz, the TM_{01} mode is lossier. This is shown in Fig. 9. As the plasma density increases further, the TE_{01} mode continues to have higher radiation loss than the TM_{01} mode. This is most likely due to the fact

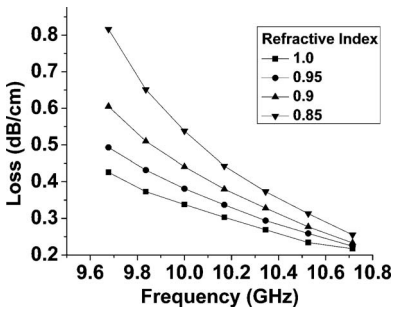

FIG. 5. TE_{01} radiation loss.

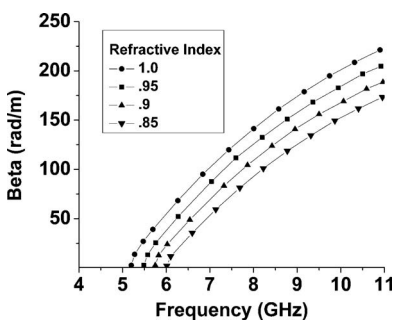

FIG. 7. Dispersion of the TM_{01} mode.

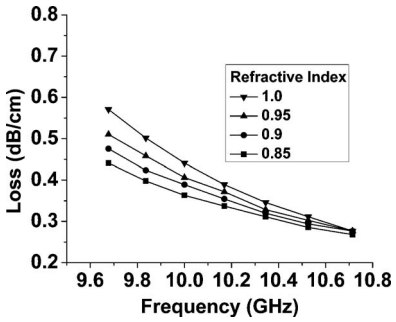

FIG. 8. TM_{01} radiation loss.

that for a given frequency, the electric and magnetic fields at the boundary of the plasma-first dielectric interface change as a function of plasma density. A larger field component at this boundary will result in higher radiative loss.

In Fig. 10, the azimuthal component of the magnetic field for the TM_{01} mode is plotted as a function of the refractive index of the core region. Again, as with the electric field for the TE_{01} mode, there is not a large difference in the field amplitude as the refractive index changes. However, the average value of the field in the cladding region decreases as the refractive index decreases, which would indicate lower radiation loss.

In Fig. 11, the dispersion of the HE_{11} mode is plotted as a function of refractive index of the core region. As with the TE_{01} and TM_{01} modes, an increase in plasma density in the core region causes an increase in cutoff frequency for the mode. Again, as with the TE_{01} and TM_{01} modes, this behavior can be understood by relating the HE_{11} mode to the TE_{11} mode of a metallic waveguide. In a hollow cylindrical metallic waveguide, the cutoff frequency is given by

$$f_c = \frac{0.293}{a\sqrt{\mu\varepsilon}}. \tag{23}$$

Figure 12 shows how the loss of the HE_{11} mode varies as a function of refractive index of the core region. As can be seen in the figure, the loss behaviors as though this mode were a combination of the behavior seen in the TE_{01} and TM_{01} modes. For frequencies less than 10.2 GHz, the loss of the HE_{11} mode decreases as the plasma density increases. At exactly 10.2 GHz, the loss of the HE_{11} mode does not change

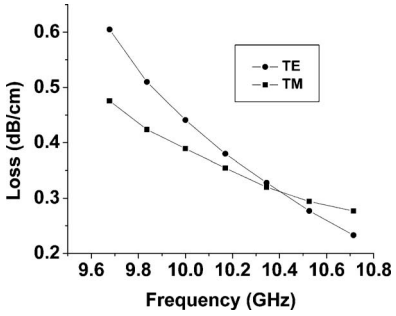

FIG. 9. TE_{01} and TM_{01} radiation loss comparison.

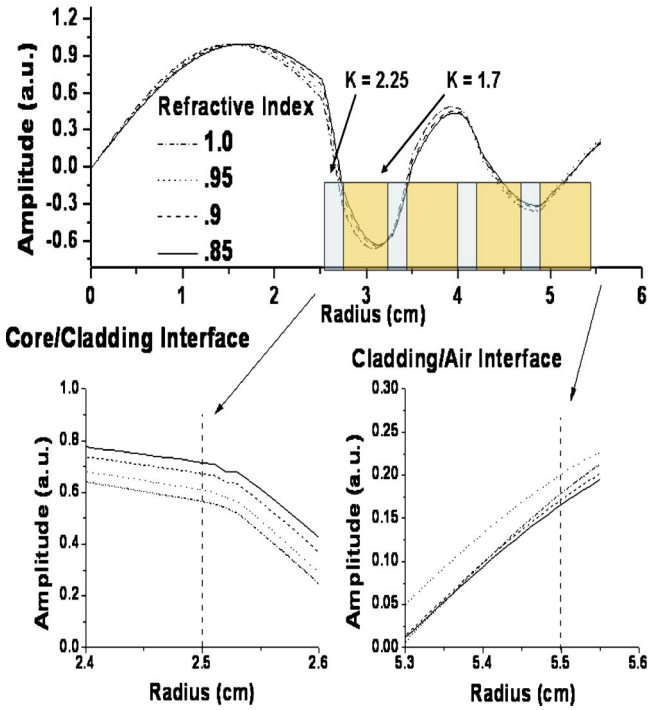

FIG. 10. (Color online) TM_{01} azimuthal magnetic field amplitudes. The lower plots show a magnified view of the core/first cladding layer interface and the last cladding layer/air interface. The dielectric layers are indicated in color and their relative permittivity values are given.

as the plasma density changes. For frequencies higher than 10.2 GHz, the loss of the HE_{11} mode increases as the plasma density increases. Again, this behavior is explained in terms of the field structure at the plasma-first dielectric boundary. For a given frequency, the electric and magnetic fields change as the boundary as a function of plasma density, with a stronger field component resulting in higher radiative loss.

IV. SUMMARY AND CONCLUSIONS

We have shown that a plasma-filled Bragg waveguide can be used to propagate relatively loss-free modes in the GHz portion of the spectrum. With the proper selection of cladding materials and thicknesses for the Bragg waveguide, dispersion and loss characteristics are calculated that compare favorably to optical Bragg fibers. The presence of a collisionless unmagnetized plasma in the core region increases the cutoff frequencies of each propagating mode. The

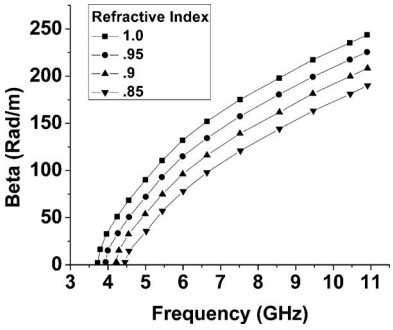

FIG. 11. Dispersion of the HE_{11} mode.

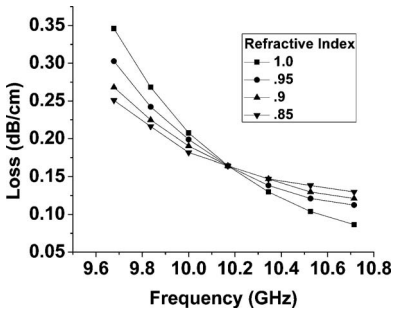

FIG. 12. HE_{11} radiation loss.

plasma also affects the loss characteristics of each mode by increasing the loss seen in the TE_{01}, and decreasing the loss in the TE_{01} mode. The HE_{11} mode experiences a superposition of those two behaviors: For frequencies lower than 10.2 GHz, the addition of a plasma decreases loss in the mode. For frequencies higher than 10.2 GHz, the plasma causes an increase in radiation loss.

ACKNOWLEDGMENTS

The authors would like to acknowledge helpful discussions with R. C. Woods. The authors would also like to thank A. Jandl for assisting with the numerical calculations.

[1]P. Yeh, A. Yariv, and E. Marom, J. Opt. Soc. Am. **68**, 1196 (1978).
[2]S. Johnson, M. Ibanescu, M. Skorobogaity, O. Weisberg, T. Engeness, M. Soljacic, S. Jacobs, J. D. Joannopoulos, and Y. Fink, Opt. Express **9**, 748 (2001).
[3]A. Argyros, Opt. Express **10**, 1411 (2002).
[4]Y. Fink, D. J. Ripin, S. Fan, C. Chen, J. D. Joannopoulos, and E. L. Thomas, J. Lightwave Technol. **17**, 2039 (1999).
[5]M. Ibanescu, Y. Fink, S. Fan, E. L. Thomas, and J. D. Joannopoulos, Science **289**, 415 (2000).
[6]J. G. Fleming, S. Y. Lin, and R. Hadley, in Proceedings of the Solid-State Sensor Actuator and Micro-Systems Workshop, Hilton Head, SC (2002), p. 173 (unpublished).
[7]S. Ramo, J. Winnery, and T. Van Duzer, *Fields and Waves in Communication Electronics*, 3rd ed. (Wiley, New York, 1994), pp. 428–432.
[8]X. Yu and A. Yariv, Opt. Express **11**, 1039 (2003).
[9]C. Balanis, *Advanced Engineering Electromagnetics* (Wiley, New York, 1989), pp. 116–121.
[10]M. Afsar and K. Button, IEEE Trans. Microwave Theory Tech. **83**, 217 (1983).